Mineralium Deposita (2023) 58:1191–1210
https://doi.org/10.1007/s00126-023-01176-w

ARTICLE

Alpine eclogite-facies modification of Li-Cs-Ta pegmatite from the Wolfsberg lithium deposit, Austria

William Keyser[1] · Axel Müller[1] · Ralf Steiner[2] · Muriel Erambert[3] · Magnus Kristoffersen[3] · Thomas Unterweissacher[2]

Received: 1 March 2022 / Accepted: 6 April 2023 / Published online: 19 April 2023

Abstract

The Wolfsberg lithium deposit in Austria is one of the largest Li-Cs-Ta pegmatite resources in Europe. The deposit is part of the Austroalpine Unit Pegmatite Province in the Eastern Alps that formed during the high-temperature, low-pressure Permian extensional event and was subsequently overprinted by Cretaceous eclogite-facies metamorphism during the Alpine orogeny. The two pegmatite types distinguished at the deposit, amphibolite hosted-(AHP) and mica schist hosted-(MHP) pegmatite, consist of quartz, albite, K-feldspar, muscovite and spodumene with accessory apatite, beryl and columbite. Both pegmatite types have similar peraluminous granitic compositions and element distribution patterns. However, the AHP contains higher Li and Cs concentrations. Both pegmatite types display LREE-enriched/HREE-depleted chondrite-normalized REY patterns that suggest derivation from partial melting of basement mica schist during the Permian HT/LP extensional event. The Alpine metamorphism more strongly affected the MHP relative to the AHP, resulting in recrystallization of primary assemblages by metamorphic assemblages with lower rare-metal concentrations, and development of a strong foliation, during which (re) mobilized elements (e.g., Li, Cs) were concentrated along localized shear zones. Recognition of element remobilization in MHP associated with metamorphic overprinting may bear important implications towards mineral exploration for Li-Cs-Ta pegmatite in other strongly metamorphosed terranes.

Keywords Wolfsberg lithium deposit · LCT pegmatite · Spodumene · Trace element geochemistry · Anatexis · Eclogite-facies metamorphism

Introduction

Spodumene-bearing lithium-cesium-tantalum (LCT; Černý and Ercit 2005)-type pegmatite represents the most important hard rock lithium resource on a global scale (Kesler et al. 2012), besides hosting a suite of other important rare-metal resources including cesium, tantalum, tin and beryllium (London 2008). Although LCT pegmatite has a worldwide distribution (Kesler et al. 2012; Shaw 2021), it often occurs as dike-like bodies previously considered too small for economic exploitation, with few exceptional LCT pegmatite occurrences contributing significantly to world lithium production (e.g., Greenbushes, Western Australia; 119.41 Mt @ 2.42 wt.% Li_2O; Sweetapple 2017). Europe has more than 500 hard-rock lithium occurrences (Gourcerol et al. 2019); the largest LCT pegmatite deposits occur in Ukraine (Nadiya, 65 Mt @ 1.12% Li_2O; Stankovaskoe, 36.15 Mt @ 1.3% Li_2O) and Portugal (Mina do Barroso, 23.5 Mt @ 1.02% Li_2O). However, the European Union only produces 1–2% of the global lithium resources (Kavanagh et al. 2018).

The Wolfsberg lithium deposit (Carinthia, Austria) is the third largest lithium pegmatite resource in Europe, with estimated resources (measured + indicated + inferred) of 12.88 Mt @ 1.0% Li_2O (European Lithium Limited 2021). The deposit is part of the Austroalpine Unit Pegmatite Province (AUPP) in the Eastern Alps (Göd 1989; Knoll et al. 2023).

Editorial handling: G. Beaudoin

✉ William Keyser
william.keyser@nhm.uio.no

[1] Natural History Museum, University of Oslo, P.O. Box 1172, Blindern, Oslo 0318, Norway

[2] GEO-Unterweissacher GmbH, Regio-Tech 1, Hochfilzen 6395, Austria

[3] Department of Geosciences, University of Oslo, P.O. Box 1047, Blindern, Oslo 0316, Norway

Pegmatite bodies throughout the AUPP exhibit variable lithium + rare-metal enrichment, however their emplacement ages are largely tied to the same Permian tectonomagmatic event (Schuster and Stüwe 2008). Genetic models for pegmatite are debated. Göd (1989) and Mali (2004) proposed pegmatite formation by fractional crystallization from a larger parent pluton. However, in the absence of strong field evidence supporting a genetic relationship between plutons and pegmatite, several authors have suggested that pegmatite is the melt product of Al-rich metapelite during the Permian event (Thöni and Miller 2000; Habler et al. 2007; Konzett et al. 2018a; Knoll et al. 2018, 2023). Recent melt experiments (Konzett et al. 2018b), fluid inclusion studies (Krenn et al. 2021) and thermodynamic modeling (Knoll et al. 2023) support an anatectic origin for pegmatite throughout the AUPP.

Detailed mineralogical and geochronological studies have been carried out on pegmatite in various localities throughout the AUPP with the aim of better understanding the timing and nature of pegmatite emplacement (e.g., Konzett et al. 2018a; Knoll et al. 2018, 2023). This study uses new petrographic observations, and mineral and whole-rock chemical data to characterize the spodumene pegmatite at the Wolfsberg deposit. The main objective is to understand variability in pegmatite mineralogy and chemistry as they relate to the amphibolite and mica schist host rocks and what implications these may carry towards understanding pegmatite formation and lithium mineralization. This study also presents an opportunity to evaluate the impact of eclogite-facies metamorphism on element remobilization following pegmatite emplacement. Such information may carry larger implications about other pegmatite bodies throughout the AUPP and LCT pegmatite deposits elsewhere.

Regional and deposit geology

Regional geological setting

The Wolfsberg deposit is located in the Koralpe region of the central Eastern Alps (Fig. 1A). The Koralpe is part of the Saualpe-Koralpe Complex, which is one of several lithostratigraphic complexes within the Koralpe-Wölz Nappe System of the polymetamorphic Austroalpine Unit nappe stack. The dominant lithologies of the Saualpe-Koralpe Complex are kyanite-bearing paragneiss and garnet-bearing mica schist with intercalations of eclogite, amphibolite, quartzite and marble (Miller et al. 2005). Magmatic lithologies present within the region include MORB-type metagabbro (247–255 Ma; Miller and Thöni 1997), granite (i.e., the Wolfsberg granitic orthogneiss, 258 ± 11 Ma; Morauf 1980) and leucogranite (250.4 ± 5.3 Ma; Knoll et al. 2018), and late Permian to Triassic spodumene-free and spodumene-bearing pegmatite (Heede 1997; Thöni and Miller 2000; Thöni and Miller 2010; Knoll et al. 2018).

The dominant metamorphic imprints recognized in the region are attributed to the Permian event and the Cretaceous Alpine orogeny. During the Permian event, lithospheric extension along the western embayment of the Neotethys Ocean was accompanied by basaltic underplating, which led to high-temperature, low-pressure metamorphism up to granulite-facies throughout the Austroalpine Unit (Schuster and Stüwe 2008). Partial melting of metasedimentary rocks at lower crustal levels led to emplacement of granitoid and pegmatite at middle to upper crustal levels throughout the AUPP at amphibolite- to greenschist-facies conditions (Knoll et al. 2023). The Cretaceous Alpine orogeny involved an intracontinental subduction to collision process during closure of the Meliata Ocean (Schmid et al. 2004), leading to variable greenschist- to eclogite-facies metamorphism throughout the Austroalpine Unit. Eclogite-bearing units in the Saualpe-Koralpe Complex are under- and overlain by basement units of lower metamorphic grade indicating an inverted metamorphic gradient such that they resemble the core of a recumbent fold within the extrusion wedge (Schmid et al. 2004).

Pegmatite within the AUPP is predominantly Permian to Triassic in age (Schuster et al. 2001; Schuster and Stüwe 2008). Exceptions include Ordovician pegmatite related to crustal melting during a 'Caledonian' magmatic event (Thöni and Miller 2004; Gangl et al. 2005; Tropper et al. 2016), late Devonian pegmatite associated with magmatism early in the Variscan orogeny (Mandl et al. 2018), and Cretaceous pegmatite emplaced during decompression melting at the end of the Alpine orogeny (Thöni and Miller 2010). Most of the pegmatite bodies are simple and consist of quartz + feldspar + muscovite assemblages. However, a small number of these are Nb–Ta-Sn-bearing spodumene pegmatite, including the most economically important Wolfsberg pegmatite.

The Wolfsberg lithium deposit

Earlier studies on pegmatite at the Wolfsberg deposit were conducted by Göd (1989) and Niedermayr and Göd (1992) and are summarized below. The Wolfsberg deposit occurs within the northern limb of a WNW-ESE-striking anticline structure ('Wolfsberg anticline,' Göd 1989) that dips ~ 60° to the NNE and was developed during regional deformation associated with the Alpine metamorphism (Fig. 1B). The area is characterized by mica schist and eclogite-amphibolite (amphibolite hereafter), with meter-thick intercalations of the former found in the latter, and decimeter-scale graphite and marble layers present within either lithology. The main pegmatite-hosting mica schist unit dips beneath the pegmatite-hosting amphibolite unit. The mica schist assemblages

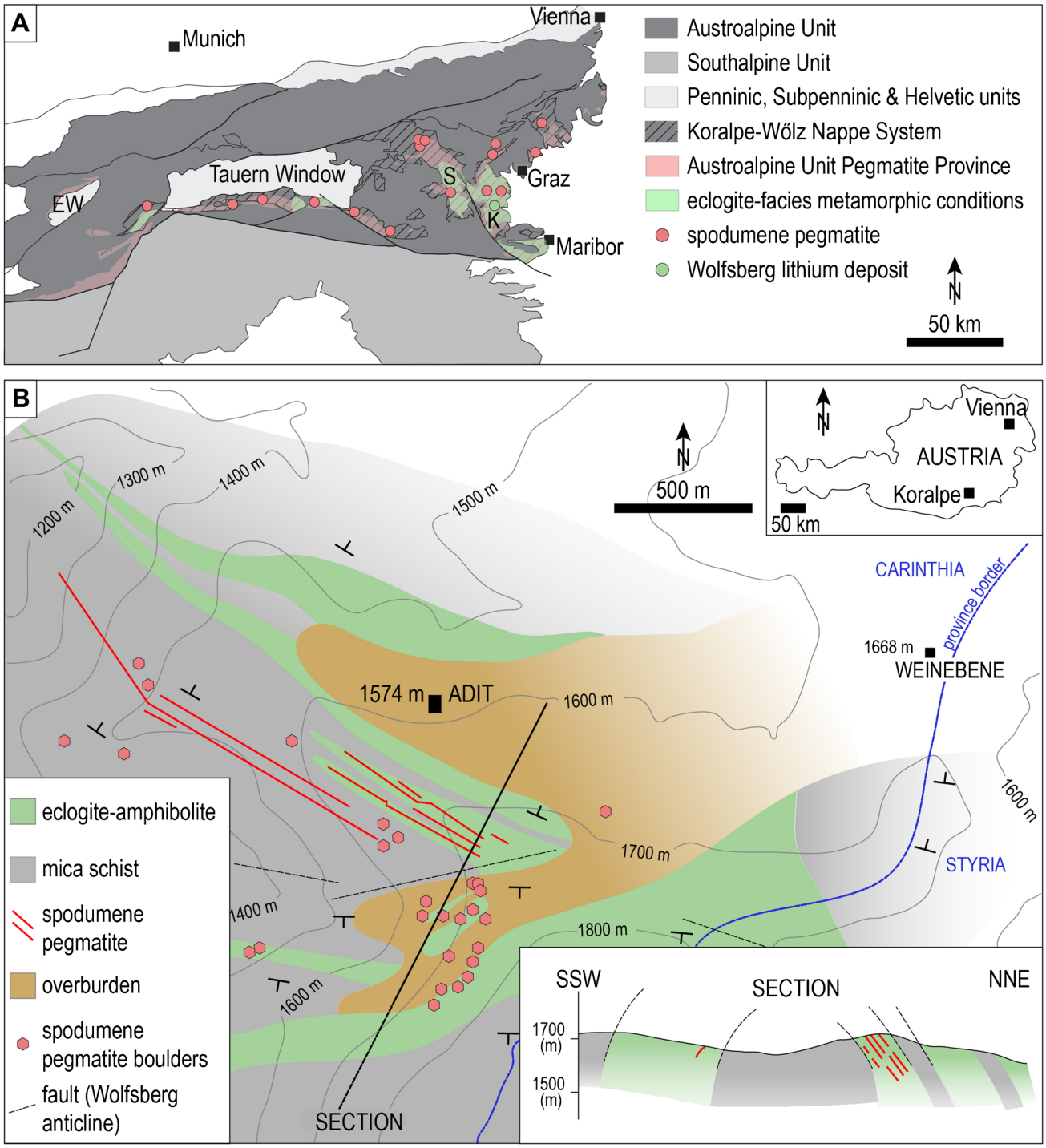

Fig. 1 **A** Simplified tectonic map of the Eastern Alps (after Konzett et al. 2018a) showing extent of the high-pressure Koralpe-Wölz Nappe System, the Austroalpine Unit Pegmatite Province with emphasis on areas metamorphosed at eclogite-facies conditions, occurrences of spodumene-bearing pegmatite (after Knoll et al. 2018) and location of the Wolfsberg deposit. Abbreviations: EW-Engadine Window; K-Koralpe; S-Saualpe. **B** Geological map of the Wolfsberg deposit after Göd (1989). Eclogite-facies conditions in (**A**) sourced from https://geolba.maps.arcgis.com/apps/webappviewer/index.html?id=ef8095943a714d7893d41f02ec9c156d

consist of muscovite + garnet + biotite + kyanite. Kyanite can measure up to centimeter-scale and displays textural features that indicate the pseudomorphic replacement of pre-existing andalusite. The amphibolite consists of amphibole + plagioclase + quartz ± garnet ± pyroxene, with calcite present as a primary component. When present, pyroxene

shows symplectic textures with extensive replacement by amphibole. Minor strata-bound scheelite is found within amphibolite.

Pegmatite occurs as roughly NW-SE-striking dikes hosted within the mica schist and amphibolite and is concordant with the foliation of the host rock. The dikes have been traced over a length of 1,300 m and to a depth of 350 m, with an average thickness of 2 m, but can reach up to 5 m in width. The pegmatite generally lacks zoning and displays sharp contacts with the host rock. However, amphibolite-hosted pegmatite displays internal irregular-shaped aplitic domains and a ~ 10–20 cm spodumene-poor aplitic border along dike margins, with a contact aureole of up to 50 cm characterized by biotitization of the host amphibolite and formation of holmquistite, tourmaline and garnet. Irrespective of host rock, pegmatite consists of quartz + feldspar + muscovite + spodumene and a range of other accessory minerals. The modal abundance of spodumene is higher in amphibolite-hosted pegmatite than in mica schist-hosted pegmatite, resulting in a ~ 0.5 wt.% higher Li_2O whole-rock composition (Göd 1989). As both pegmatite types are believed to have crystallized from the same highly fractionated melt, differences between them are attributable to melt reactivity with different host rocks and degree of metamorphic overprint resulting from different host rock competence (Göd 1989).

Geochronological data for pegmatite at the Wolfsberg deposit are limited. Zircon from pegmatite yielded a U-Pb age of 240 ± 1.5 Ma that was interpreted to represent the timing of emplacement (Heede 1997). Thöni and Miller (2000) obtained spodumene-whole rock isochron ages of 242.8 ± 1.7 and 238.5 ± 2.6 Ma for pegmatite samples that were also suggested to represent the timing of pegmatite emplacement. However, Sm-Nd mineral isochron ages of 87 and 65 Ma from the aplitic border zone of an amphibolite-hosted pegmatite by Thöni and Miller (2000) were interpreted to reflect local eclogite-facies remobilization and recrystallization of the Permian protolith during the Alpine orogeny.

Methodology

Sampling

The sample suite was collected from selected drill cores intersecting representative pegmatite types at the Wolfsberg deposit. To assess the impact of possible zoning within individual pegmatite dikes or host rock interaction, samples from larger pegmatite dikes (> 2 m in thickness) were taken proximal to upper and lower contacts with the host rock and within dike centers. Samples of the host mica schist are also included due to its possible genetic relationship to pegmatite (Konzett et al. 2018b; Schuster et al. 2019; Krenn et al. 2021). Although not discussed in this study, whole-rock chemical data for amphibolite samples are included in spider diagrams for comparison. Mica schist and amphibolite samples were collected from the tunnel walls perpendicular to pegmatite strike at increasing intervals from 0.1 to > 100 m.

Analytical methodology

One hundred and fourteen samples were assayed for whole-rock chemistry by ALS Minerals (Loughrea, Ireland) to determine average rare-metal contents, which was provided by GEO-Unterweissacher GmbH. An additional forty-five samples were analyzed by Activation Laboratories Ltd. (Ontario, Canada). Further details on whole-rock analytical methodology with detection limits and whole-rock data are provided in Electronic Supplementary Material (ESM) Tables S1 and S2, respectively.

Petrographic characterization of the samples was carried out on polished thick (300 µm)- and thin (100 µm)-sections (2.5 × 5 cm) using a Hitachi S-3600 scanning electron microscope (SEM) with high-resolution back-scattered electron (BSE) imaging capabilities equipped with a Bruker XFlash® 5030 energy dispersive X-ray detector (EDX), housed at the Geo Laboratory at the Natural History Museum, University of Oslo, Norway.

Major and minor element analysis of selected minerals was performed using a Cameca SX100 Electron Probe Micro-Analyzer (EPMA) equipped with five wavelength-dispersive X-ray spectrometers. Analytical conditions for microprobe analysis were 15 kV acceleration voltage with a 15 nA (silicates) or 20 nA beam current and a focused electron beam. Mineral trace element analysis was conducted using a Bruker Aurora Elite Q-ICPMS with a Cetac LSX-213 G2 + laser microprobe. Trace elements were measured using a laser frequency of 20 Hz and a spot size of 50 µm. Both instruments are housed at the Department of Geosciences, University of Oslo, Norway. Additional information on analytical methods including standards and minimum detection limits (mdl) is provided in ESM Tables S3 and S4.

The studied pegmatite

The study focuses on the two main pegmatite types at the Wolfsberg deposit that are referenced according to their amphibolite and mica schist host rocks. Amphibolite-hosted pegmatite (AHP; Fig. 2A, B) displays coarse-grained magmatic textures and consists of greyish spodumene crystals (up to 5 cm) and dark mica flakes (mm-scale) within a matrix of white feldspar and greyish quartz. The AHP

also has ~ 10 cm spodumene-free aplitic border zones along margins (Fig. 2C) and irregular aplitic domains interpreted as albitization products (Fig. 2D). These consist mostly of albite, muscovite, quartz, and in the border zones, tourmaline. Mica schist-hosted pegmatite (MHP; Fig. 2 E, F) is generally fine-grained and displays a distinct gneissic appearance resulting from alternating quartz- and feldspar-rich bands with dark aligned micas (Fig. 2F).

Petrography and mineralogy

Amphibolite-hosted pegmatite

The AHP contains mineral assemblages consisting of quartz, feldspars (mostly albite but also K-feldspar), muscovite and spodumene, all of which can be found as inclusions in, and sharing equilibrium grain boundaries with, one another. Grains of near end-member albite and K-feldspar are anhedral and measure up to several millimeters in size, however the latter displays perthitic textures in grain cores (Fig. 3A). Muscovite occurs as randomly oriented mm-scale flakes with either straight or embayed margins and typically has cleavages lined with apatite (Fig. 3A, B). Muscovite + quartz symplectites are common along grain boundaries of K-feldspar and muscovite (Fig. 3B). Spodumene occurs as mm-scale euhedral to subhedral grains (Fig. 3A, B), and spodumene-quartz intergrowth textures along grain margins are common. Cookeite is commonly observed replacing spodumene along grain boundaries and fractures (Fig. 3B). A typical feature in the AHP is the presence of oriented fine-grained platy albite replacing K-feldspar and spodumene (Fig. 3C), which in turn can be crosscut by albite veinlets, as seen in cathodoluminescence images (Fig. 3D). Such albite is associated with various phosphate minerals.

Accessory minerals are abundant in the AHP and include a diverse suite of phosphates, beryl, columbite group minerals (CGM), tourmaline, zircon, uraninite, cassiterite and graphite. The most common phosphate mineral is Mn-rich apatite, which is subhedral and measures several hundreds of microns in size and commonly occurs with other accessory minerals such as beryl (Fig. 3E), uraninite, CGM, and other phosphates such as triphylite, fairfieldite, beryllonite, tiptopite and montebrasite (Fig. 3F). Beryl forms clusters of variably-shaped grains and commonly contains inclusions of quartz, apatite, CGM, albite and K-feldspar. Compositional zoning is rare in beryl but occurs in more euhedral grains (Fig. 3G). Tourmaline in the aplitic border zones displays variable sizes and morphologies, from mm-scale subhedral grains, to fine-grained and euhedral, to interstitial. Coarse-grained tourmaline displays scalloped margins and compositional zoning with a complex inclusion suite of phosphates, including montebrasite, CGM, spodumene, cassiterite, zircon, albite, K-feldspar and quartz (Fig. 3H). Fine-grained euhedral tourmaline lacks zonation and contains only quartz inclusions (Fig. 3I), whereas tourmaline lacking both inclusions and zoning occurs interstitial to albite (Fig. 3J).

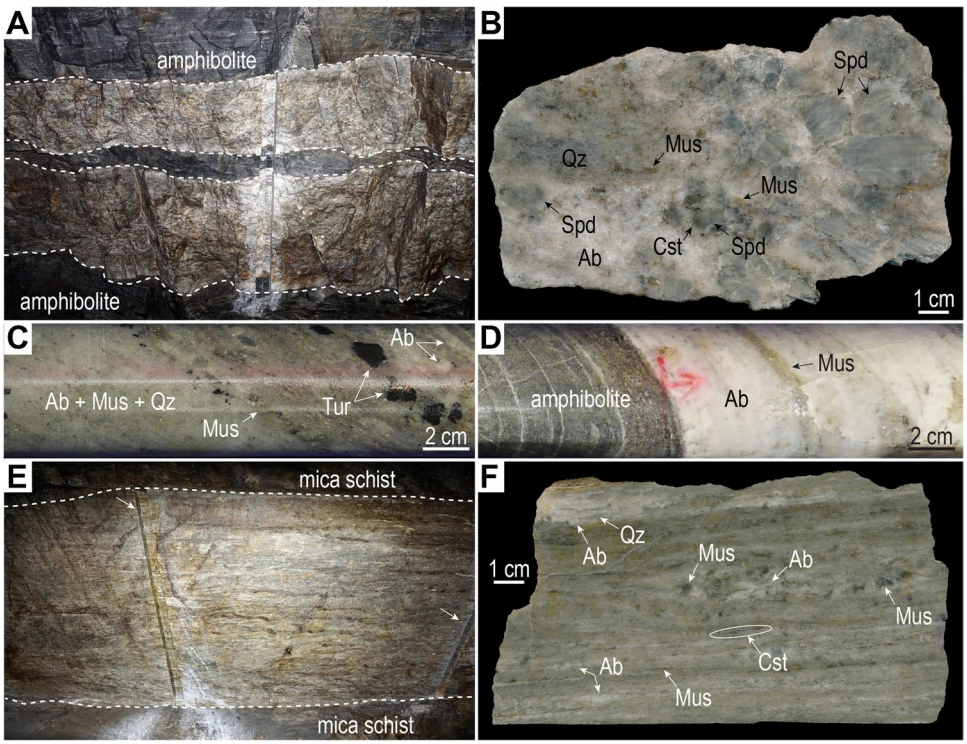

Fig. 2 Photographs of mine exposures, drill core and samples of representative pegmatite types. (**A**) A ~ 2-m-wide amphibolite-hosted pegmatite dike along the mine tunnel ceiling. (**B**) Amphibolite-hosted pegmatite specimen showing coarse-grained texture. (**C**) Border zone of amphibolite-hosted pegmatite containing muscovite, albite and tourmaline. (**D**) Aplitic (albitized) pegmatite in contact with amphibolite host rock. (**E**) A ~ 2-m-wide mica schist-hosted pegmatite along mine tunnel ceiling. White arrows show rock cuts across width of pegmatite. (**F**) Mica schist-hosted pegmatite showing gneissic texture. Abbreviations: Ab-albite; Cst-cassiterite; Mus-muscovite; Qz-quartz; Spd-spodumene; Tur-tourmaline

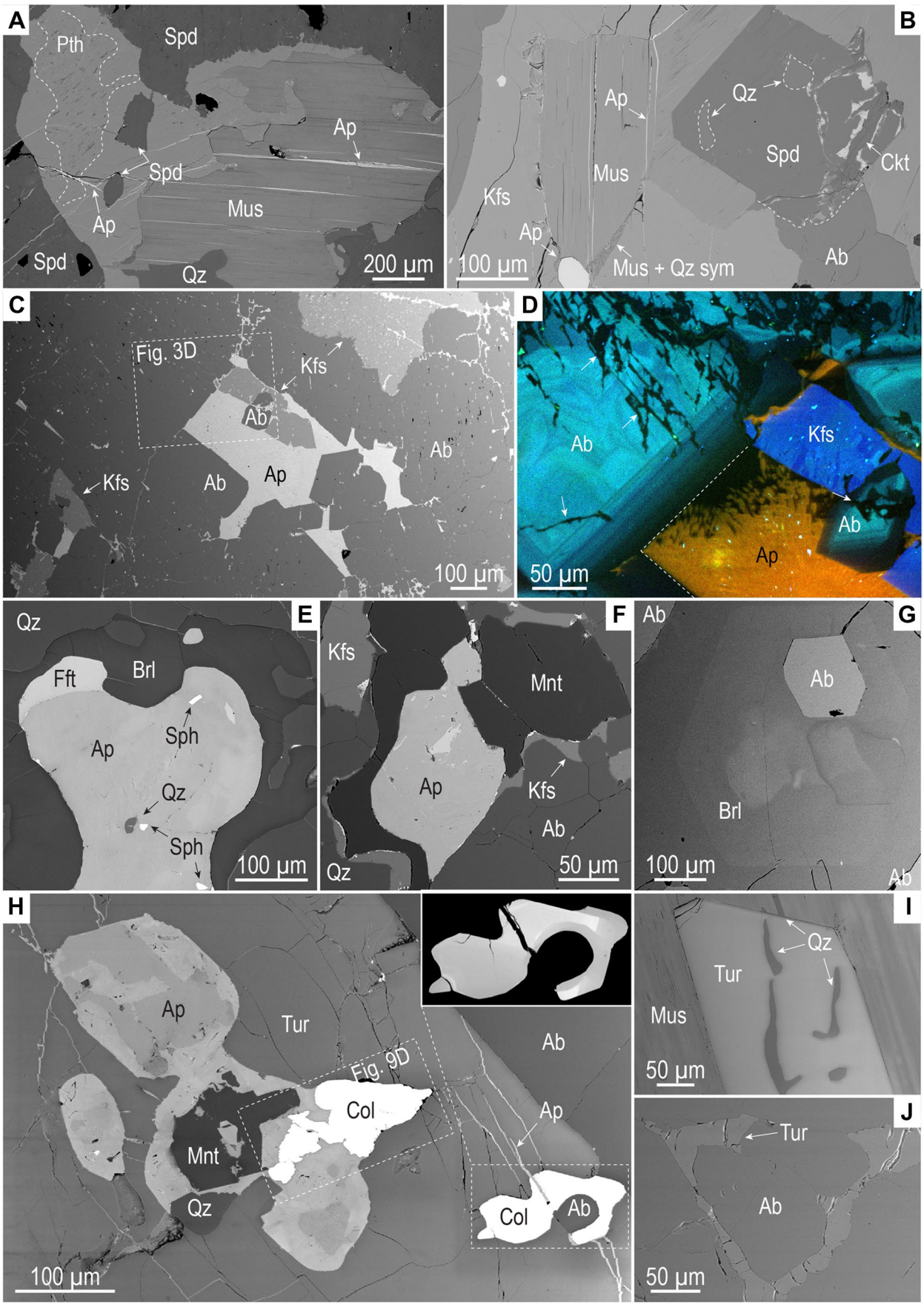
A
Pth
Spd
Ap
Spd
Mus
Ap
Spd
Qz
200 µm
B
Ap
Qz
Spd
Ckt
Mus
Kfs
Ap
100 µm
Mus + Qz sym
Ab
C
Fig. 3D
Kfs
Ab
Ab
Kfs
Ab
Ap
100 µm
D
Ab
Kfs
Ab
Ap
50 µm
E
Qz
Fft
Brl
Ap
Sph
Qz
Sph
100 µm
F
Kfs
Mnt
Ap
Kfs
Ab
Qz
50 µm
G
Ab
Ab
Brl
100 µm
Ab
H
Ap
Tur
Fig. 9D
Col
Mnt
Qz
Ab
Ap
Col
Ab
100 µm
I
Qz
Tur
Mus
50 µm
J
Tur
Ab
50 µm

◂**Fig. 3** BSE and CL images showing representative features of amphibolite-hosted pegmatite. (**A**) Coarse-grained K-feldspar with perthitic core intergrown with muscovite and spodumene. (**B**) Euhedral spodumene with muscovite and K-feldspar. Note the incipient replacement of spodumene by cookeite and formation of muscovite + quartz symplectites along the contact of K-feldspar and muscovite. (**C**) Oriented platy albite with apatite replacing K-feldspar, with inset (**D**) showing CL image of later albite veinlets (white arrows) crosscutting the platy albite. Apatite associated with (**E**) beryl and (**F**) montebrasite. (**G**) Beryl showing compositional zoning. (**H**) Coarse-grained tourmaline with quartz, phosphate and CGM (inset) inclusions and crosscut by apatite stringers. (**I**) Euhedral tourmaline with quartz inclusions, surrounded by muscovite. (**J**) Rounded albite grains with interstitial tourmaline. Abbreviations: Ab-albite; Ap-apatite; Brl-beryl; Ckt-cookeite; Col-columbite; Kfs-K-feldspar; Mnt-montebrasite; Mus-muscovite; Pth-perthite; Qz-quartz; Spd-spodumene; Sph-sphalerite; Sym-symplectite; Tur-tourmaline

Mica schist-hosted pegmatite

The MHP consists of quartz, albite, muscovite and spodumene, although relicts of earlier minerals are present (e.g., K-feldspar). Coarse-grained muscovite defines the main foliation (Fig. 4A), but fine-grained muscovite forms aggregates, overgrowths on coarser grains, or is intergrown with quartz as symplectites (Fig. 4B). Coarse-grained spodumene occurs as elongated porphyroblasts within the foliation with muscovite (Fig. 4C). Specific to the MHP is staurolite, which occurs locally as fine-grained (~ 10 µm) laths together with gahnite along spodumene margins (Fig. 4D), or as coarse-grained (> 100 µm) porphyroblasts within the foliation and as inclusions in aligned muscovite (Fig. 4E). The latter texture always contains symplectic quartz inclusions, but commonly also contains muscovite, apatite and columbite (Fig. 4E inset).

Accessory minerals in the MHP are much the same as those found in the AHP but with a high degree of alteration/deformation. Apatite is abundant and is largely replaced by, or associated with, various secondary phosphates (e.g., wolfeite, fairfieldite, beryllonite, tiptopite). Late apatite occurs as crosscutting veins and is intergrown with aligned muscovite (Fig. 4A). Euhedral beryl porphyroblasts containing aligned nano-inclusions of cordierite + quartz intergrowths can be found within the foliation (Fig. 4A, F). Cassiterite is rare and uncommonly contains aligned micro-inclusions (exsolutions?) of zoned columbite or displays compositional zoning (Fig. 4G, H). Such cassiterite is also associated with chrysoberyl that displays compositional zoning (Fig. 4H). Also rare is columbite with inclusions of zircon, albite, wodginite, uraninite and other CGM (Fig. 4I).

Mica schist

The medium-grained host mica schist is composed of muscovite, biotite, quartz, plagioclase, garnet, staurolite, kyanite, tourmaline, rutile and graphite with accessory zircon, apatite, monazite, allanite and pyrite. The rocks are characterized by a foliation defined by variably-sized muscovite, biotite, graphite and tourmaline. Almandine-rich garnet ($Alm_{60\text{-}70}$ $Sps_{0.2\text{-}2}Pyp_{11\text{-}21}Grs_{11\text{-}22}$) forms ~ 0.5-2 mm porphyroblasts that are wrapped by the external foliation and display textures suggesting multiple growth stages (Fig. 5A). An early stage of garnet growth (Grt_1) is indicated by cores rich with biotite, muscovite, quartz, plagioclase, rutile and graphite inclusion trails, which can be continuous or discontinues with the external foliation. Inclusion-poor garnet rims, irregular garnet overgrowths or inclusion-poor grains lacking zonation are representative of later garnet growth (Grt_2). Staurolite occurs as porphyroblasts or laths up to ~ 0.5 mm within the main foliation and is typically rich with quartz and graphite inclusion trails continuous with the main foliation (Fig. 5B). Kyanite is associated with staurolite and similarly occurs within the main foliation with irregular shapes (Fig. 5B). Tourmaline is abundant as rounded or elongated grains within the matrix and as inclusions in garnet rims and displays dark green graphite-rich cores and pale green rims in transmitted light (Fig. 5C).

Whole-rock geochemistry

Whole-rock data are provided in ESM Table S2. All pegmatite samples have peraluminous compositions. Pegmatite has a wide range of SiO_2 (~ 67–79 wt.%), but relatively similar concentrations of most other elements (Fig. 6). Noteworthy differences between the AHP and the MHP are the higher mean concentrations of Li_2O (0.85 wt.%), CaO (1.5 wt.%) and Na_2O (4.2 wt.%) in the AHP compared to the MHP (0.76 wt.%, 0.65 wt.% and 3.4 wt.%, respectively). Relative to pegmatite, the host mica schist has higher mean concentrations of most elements with the exception of SiO_2, Na_2O, P_2O_5 and Li_2O (0.11 wt.%) (Fig. 6). Although the geochemical properties of the amphibolite host rock will not be discussed in detail, it contains mean Li_2O content comparable to the mica schist.

On the diagram for selected elements normalized to upper continental crust (Fig. 7A), the distribution patterns for the two pegmatite types are similar and show notable enrichments in Li, Be, B, Ga, Rb, Nb, Sn, Cs and Ta. On average, the AHP contains higher concentrations of Li and Cs when compared to the MHP, which contains higher concentrations of Be, B, Sn, Th and U. The host mica schist displays element enrichments similar to those of the two pegmatite types but to a lesser degree. Chondrite-normalized REY patterns for pegmatite and mica schist are similar but differ with respect to the ΣREY, slope and magnitude of anomalies (Fig. 7B). Pegmatite and mica schist are LREE-enriched/HREE-depleted. Both the MHP and the mica schist have strong negative Eu anomalies, whereas the AHP has either

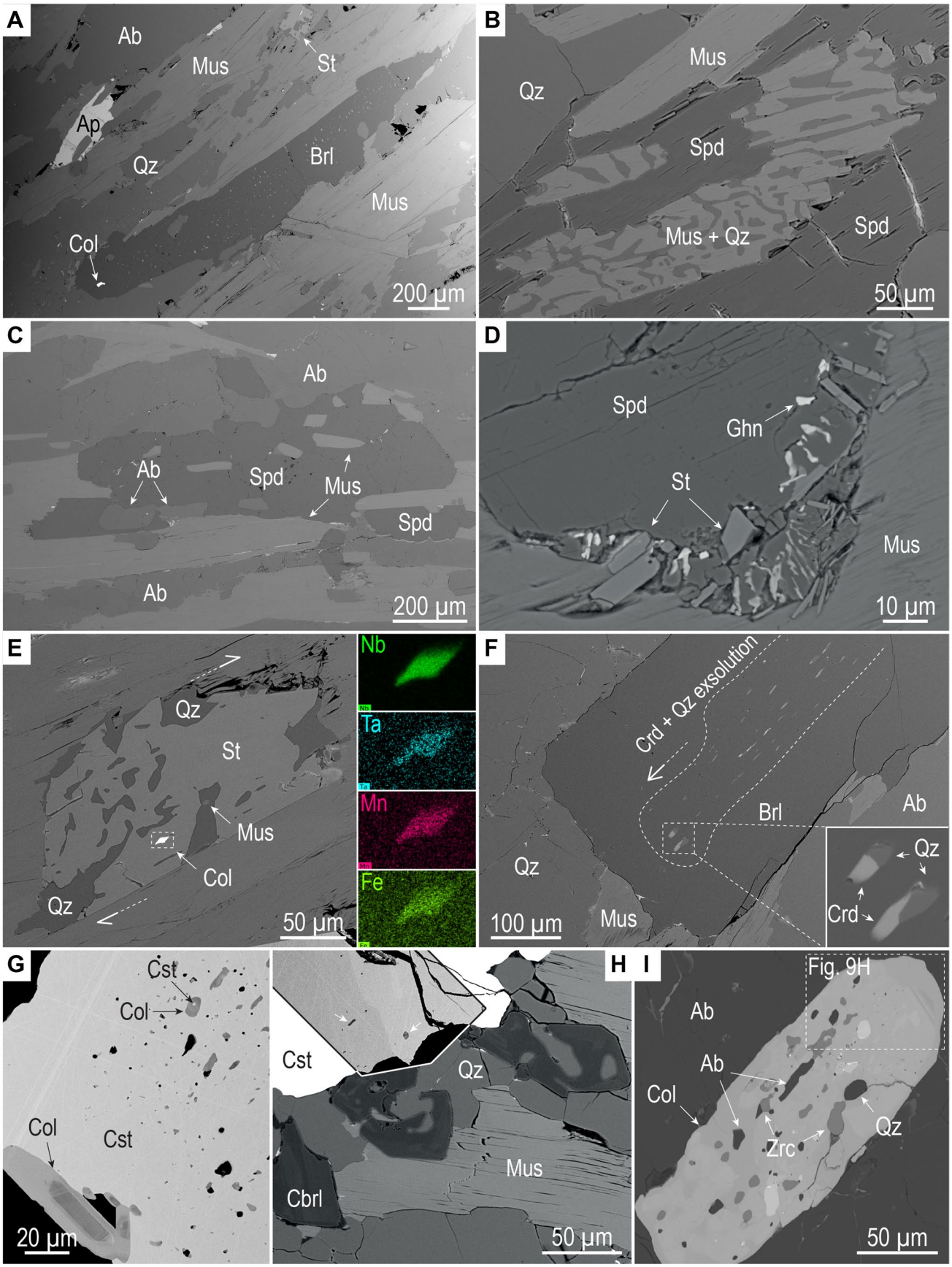
A
Ab
Mus
St
Ap
Qz
Brl
Mus
Col
200 µm
B
Mus
Qz
Spd
Mus + Qz
Spd
50 µm
C
Ab
Ab
Spd
Mus
Spd
Ab
200 µm
D
Spd
Ghn
St
Mus
10 µm
E
Qz
St
Mus
Col
Qz
50 µm
Nb
Ta
Mn
Fe
F
Crd + Qz exsolution
Brl
Ab
Qz
Mus
100 µm
Qz
Crd
G
Cst
Col
Col
Cst
20 µm
H I
Fig. 9H
Cst
Qz
Mus
Cbrl
50 µm
Ab
Ab
Col
Zrc
Qz
50 µm

◂**Fig. 4** BSE images showing representative features of mica schist-hosted pegmatite. (**A**) The main foliation showing coarse-grained muscovite, beryl, quartz, albite and staurolite. Note the fine-grained inclusions in beryl consisting of columbite and cordierite + quartz intergrowths. (**B**) Muscovite + quartz symplectites included in spodumene within the foliation. (**C**) Elongated spodumene with albite + muscovite inclusions in the foliation. (**D**) Staurolite + gahnite along margin of spodumene. (**E**) Staurolite porphyroblast included in aligned muscovite. Note the inclusions of quartz and columbite (element maps inset for clarity). (**F**) Aligned beryl porphyroblast with inclusions of aligned cordierite + quartz (inset). (**G**) Cassiterite with inclusions of aligned columbite that show compositional zoning. (**H**) Compositional zoning in cassiterite (inset) with chrysoberyl along margin, which also shows patchy compositional zoning. Columbite inclusions in inset indicated with white arrows. (**I**) Columbite with inclusions of zircon, albite and quartz as well as other CGMs (inset shown in Fig. 9H). Abbreviations: Ab-albite; Ap-apatite; Brl-beryl; Cbrl-chrysoberyl; Col-columbite; Crd-cordierite; Cst-cassiterite; Ghn-gahnite; Kfs-K-feldspar; Mus-muscovite; Qz-quartz; Spd-spodumene; St-staurolite; Tur-tourmaline; Zrc-zircon

positive or negative anomalies depending on the individual sample. The host amphibolite has consistently flat REY patterns with no distinct anomaly.

Mineral chemistry

Micas

Coarse-grained muscovite in the AHP, and aligned muscovite in the MHP, were the primary targets for EPMA (ESM Table S5). However, fine-grained symplectic muscovite intergrown with quartz in both pegmatite types (Figs. 3B and 4B) was also analyzed. Muscovite from the MHP is generally higher in Al and Na than that in the AHP, which has higher Si, Fe and Mg (Fig. 8A-C). Within individual samples, coarse-grained and aligned muscovite in the AHP and the MHP, respectively, contains higher concentrations of Si, Ti, Fe, Mg and Na than symplectic muscovite, which has higher Al and K. Figure 8A-C shows strong negative correlations on binary plots for Si versus Al^{tot} (*apfu*), $Fe^{tot} + Mg$ (*apfu*) versus Al^{tot} (*apfu*) and K/(K + Na + Rb) versus Na (*apfu*). The composition of symplectic muscovite in the AHP is similar to that of aligned muscovite in the MHP in these plots. Muscovite from the AHP has higher Si, Ti, Fe and Mg concentrations than that in the MHP, which has higher Al and Na. Muscovite from the host mica schist contains higher concentrations of Si, Ti and Mg, and lower concentrations of Al when compared to the compositional range of muscovite from pegmatite.

Muscovite from the AHP and the MHP contains comparable concentrations of most trace elements (ESM Table S6). However, muscovite from the AHP is notably enriched in Cs, Li, B, Sn and Nb relative to aligned muscovite in the MHP, which is slightly more enriched in Zn and Ta. The mean Nb/Ta ratio of muscovite from the AHP (7.2) is significantly higher than that of muscovite from the MHP (4.6). Both muscovite types have REY < 1 ppm. Plots comparing the K/Rb ratio versus various rare elements in muscovite show trends with decreasing K/Rb ratios and increasing concentrations of Cs, Li, B, Sn, Mn and Nb/Ta for the AHP, whereas aligned muscovite in the MHP shows opposite trends (Fig. 8D-I). Concentrations of Cs, Li and B are higher in muscovite from tourmaline-bearing AHP. Aligned muscovite associated with staurolite in the MHP has the highest K/Rb ratios and low concentrations of Cs, Li, B and Sn. Muscovite from the host mica schist has the lowest concentrations of Cs, Li, B, Sn and Mn, and the highest K/Rb and Nb/Ta ratios when compared to muscovite from pegmatite. It is noteworthy that the highest concentrations of Li (~ 1,030 ppm) occur in biotite from the host mica schist (Fig. 8E; ESM Table S6).

Spodumene

Spodumene composition is relatively homogenous with respect to SiO_2, Al_2O_3 and Li_2O irrespective of host rock (ESM Table S7). Other elements in low concentrations (< 1.0 wt.%) include FeO, MnO and Na_2O. Trace element analysis of spodumene within the two pegmatite types consistently measured concentrations of B, Mg, P, Ti, Cr, Mn, Zn, Ga and Sn > 10 ppm, concentrations of Be, Sc, V and Ge between ~ 1 and 10 ppm, and concentrations of Cs, Nb, Ta and Pb < 1 ppm (ESM Table S8). The ΣREY of spodumene is < 1 ppm with nearly all elements below detection. Notable differences between spodumene from the two pegmatite types are higher concentrations of Mg, P, Ti, Sn, Cs, Nb and Ta in spodumene from the AHP compared to that of the MHP, which was comparably more enriched in Mn, Sc and Zn.

Niobium-tantalum-tin minerals

Columbite group minerals in pegmatite occurs in a variety of morphologies, sizes and zoning patterns (Fig. 9). Dark and bright intensities in BSE images showing CGM zoning correspond to Nb-richer and Ta-richer compositions, respectively. Four textures of CGM were observed in the AHP and include: (1) rounded grains > 100 µm in size with Ta-rich cores, Nb-richer mantles and Ta-rich rims (Fig. 9A); (2) rod-shaped grains with Nb-rich cores and mottled rims indicating resorption (Fig. 9B), (3) grains that lack obvious compositional zoning and are always associated with Mn-rich apatite and uraninite (Fig. 9C); (4) irregularly-shaped grains with patchy zoning found as inclusions in tourmaline in the aplitic border zone (Figs. 3H and 9D).

Rod-shaped CGM grains are the most common texture within the MHP. The grains often display zoning from

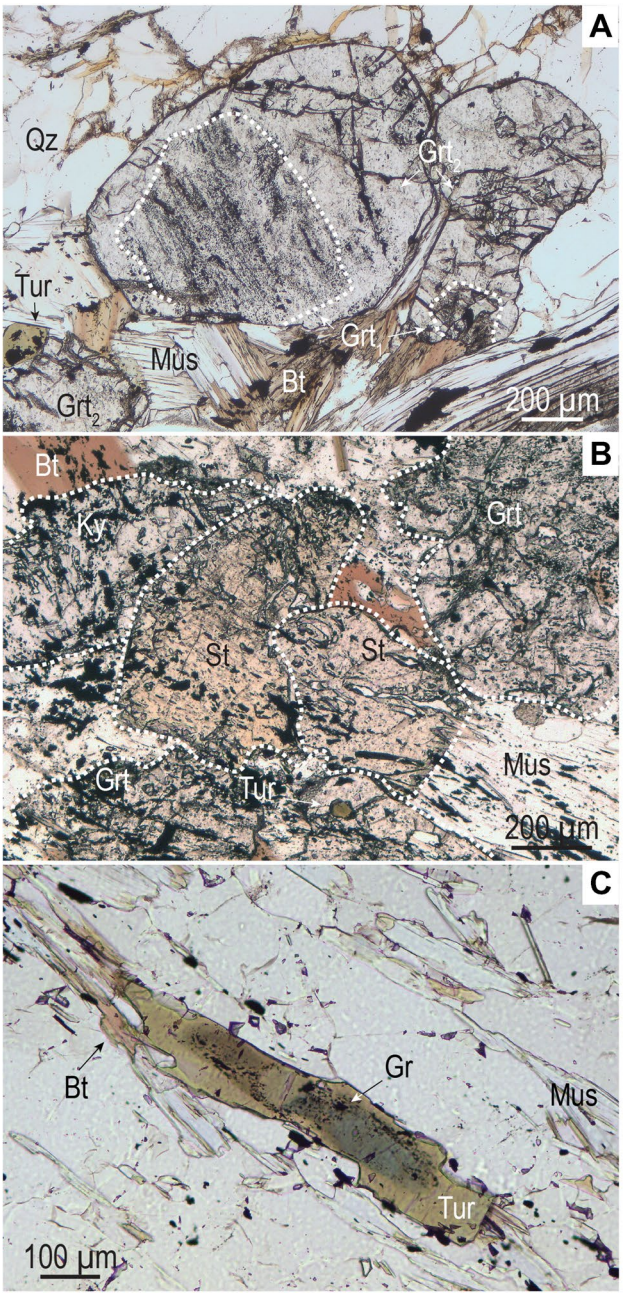

Fig. 5 Optical images from host mica schist. (**A**) Garnet showing inclusion-rich core (Grt_1) and inclusion-poor rim (Grt_2). (**B**) Textural relationship between staurolite, kyanite, garnet and muscovite, all showing abundant graphite inclusions. (**C**) Elongated tourmaline with graphite-rich bluish core and graphite-poor pale green rim. Abbreviations: Bt-biotite; Gr-graphite; Grt-garnet; Ky-kyanite; Mus-muscovite; Qz-quartz; St-staurolite; Tur-tourmaline

Nb-rich cores to Ta-rich rims (Figs. 4G and 9E). Rarely, CGM can display complex zoning patterns where both sectorial and oscillatory zoning occur within the same grain (Fig. 9F). Columbite inclusions in aligned muscovite display inverse zoning from Ta-rich cores to resorbed mantles and Nb-rich overgrowths (Fig. 9G). Similar Nb-rich overgrowths can also be found on columbite showing complex zoning patterns and a diverse suite of inclusions as described above (Figs. 4I and 9H). It is important to note that fine-grained needle-like columbite is also commonly found as inclusions in aligned muscovite or porphyroblastic staurolite within the foliation (Fig. 4E).

The compositional range of the various CGM textures is narrow with respect to X_{Mn} ($Mn/(Mn+Fe_{tot}^{2+})$; 0.25–0.53), whereas the X_{Ta} ($Ta/(Ta+Nb)$) range is much wider (0.06–0.56) (Fig. 9I; ESM Table S9). Columbite from the AHP generally has lower X_{Mn} than that of the MHP, with the exception of columbite with uraninite and apatite associations. Columbite inclusions in cassiterite from the MHP has the highest X_{Ta} values. In general compositional zoning in columbite corresponds to increasing X_{Ta} values from core towards rim, with the exception of columbite from the MHP showing inverse zoning or overgrowths (Fig. 9G, H). Noteworthy minor elements present within the CGM include MgO, TiO_2, SnO_2, Sc_2O_3 and WO_3. Columbite associated with uraninite from the AHP has the highest concentrations of TiO_2, Sc_2O_3 and WO_3, all of which are positively correlated with one another. Both pyrochlore-group minerals and wodginite, only found as inclusions in complexly zoned columbite (Figs. 4I and 9H), have the highest X_{Ta} values, with the latter also containing ZrO_2 (ESM Tables S9 and S10).

Staurolite

As staurolite was only found in the MHP, its composition is compared with that in the host mica schist. Staurolite in both lithologies is iron-rich ($Fe/(Fe+Mg) = 0.81–1.0$; Fig. 10, ESM Table S12). However, staurolite within the MHP contains higher concentrations of Al_2O_3, ZnO and MnO than that in the host mica schist, which has higher FeO, MgO and TiO_2. Noticeable differences are also observed between the compositions of fine-grained staurolite inclusions in spodumene and staurolite porphyroblasts within the foliation of the MHP, where the former contains higher ZnO, Na_2O and TiO_2 and lower FeO than the latter. Staurolite from the MHP is significantly enriched in Li (~4,550 ppm), Ge, Nb, Sn and Ta compared to that in the mica schist (Li ~ 2,800 ppm), which is enriched in V, Cr and Co relative to that in the MHP (ESM Table S13).

Tourmaline

All tourmaline from the AHP and the mica schist belongs to the alkali group and contains higher Na + K values (0.38–0.91) than Ca (< 0.15) and X-site vacancy values (0.06–0.61) (Fig. 11A; ESM Table S14). Tourmaline compositions from both lithologies belong to the schorl-dravite

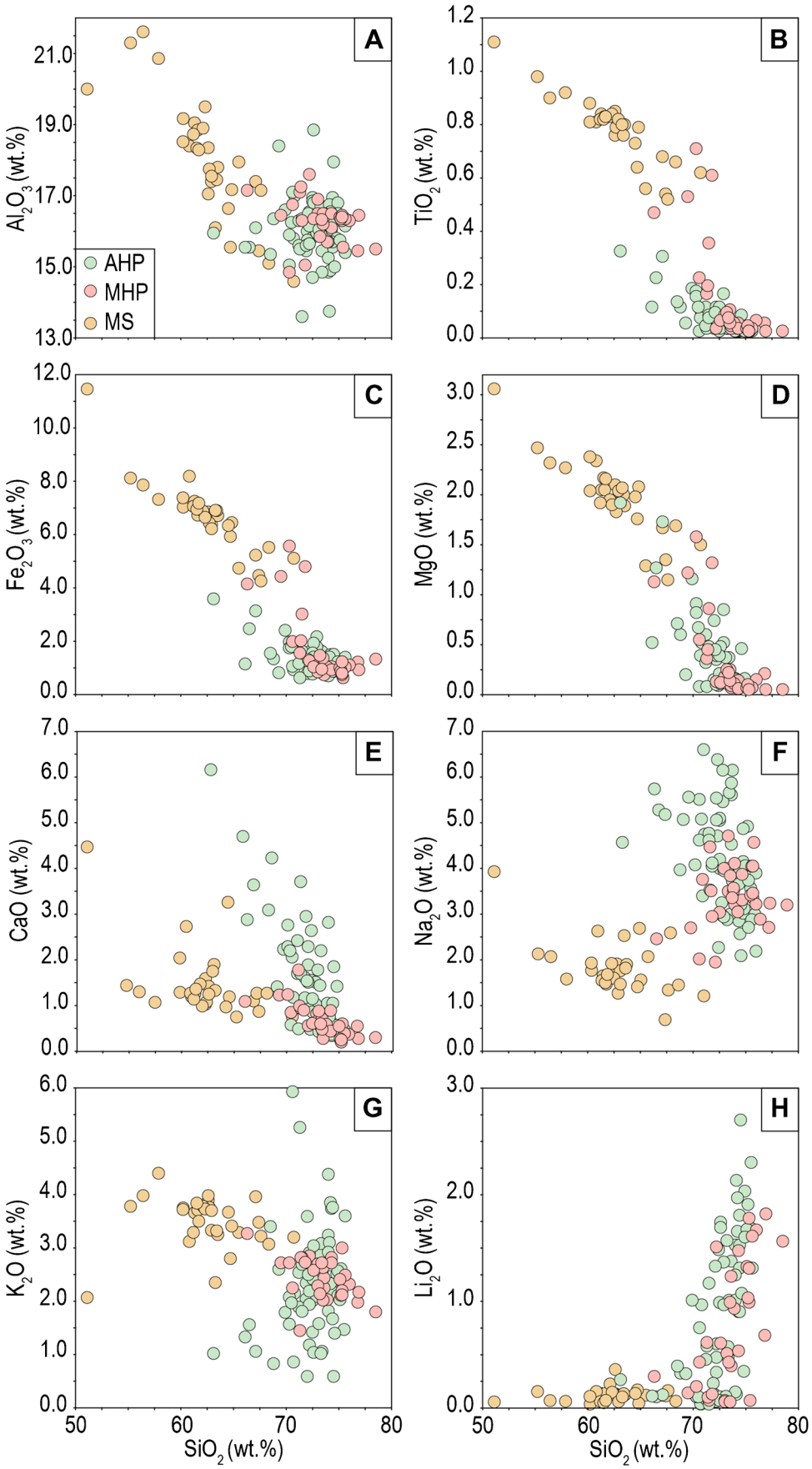

Fig. 6 Whole-rock compositional data (wt.%) for pegmatite showing SiO_2 plotted against (**A**) Al_2O_3; **B**) TiO_2; (**C**) Fe_2O_3; (**D**) MgO; (**E**) CaO; (**F**) Na_2O; (**G**) K_2O; and (**H**) Li_2O. Abbreviations: AHP-amphibolite-hosted pegmatite; MHP-mica schist-hosted pegmatite; MS mica schist

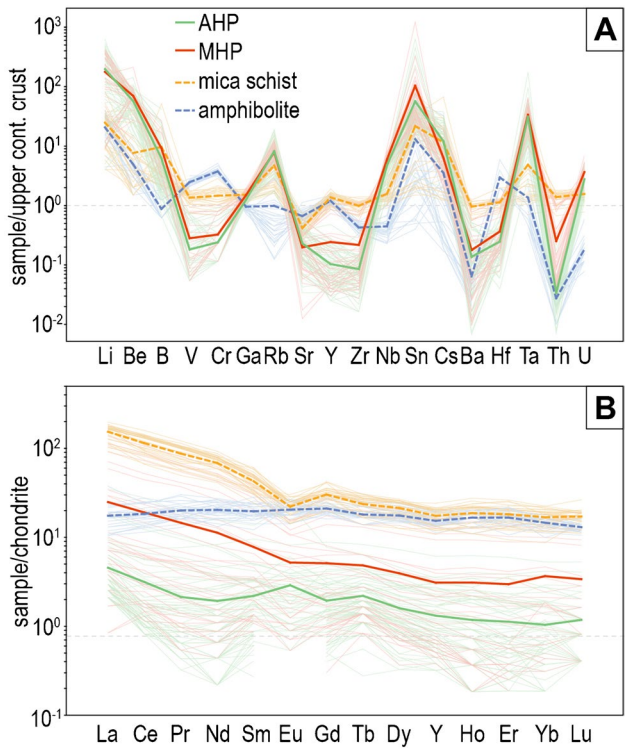

Fig. 7 **A** Upper continental crust-normalized (after Rudnick and Gao 2004) trace element plot and **B** chondrite-normalized (after McDonough and Sun 1995) REY fractionation diagram for pegmatite and mica schist. Thick lines represent lithology averages. Abbreviations: AHP-amphibolite-hosted pegmatite; MHP-mica schist-hosted pegmatite

solid solution series (Fig. 11B). However, tourmaline from the AHP is schorlitic (X_{Fe} (Fe/Fe + Mg) = 0.80–0.91) with mean ZnO and MnO of 0.29 and 0.19 wt.%, respectively, whereas tourmaline from mica schist is dravitic (X_{Fe} = 0.18–0.43). In coarse-grained tourmaline from the AHP, increasing Al (*apfu)* from core to rim is accompanied by decreasing Mg (*apfu)* and Ti (*apfu)*, whereas Fe (*apfu)* decreases from core to mantle, then increases towards rim. Blue cores in tourmaline from mica schist (Fig. 5C) correspond to higher FeO and TiO_2 concentrations.

Tourmaline from the AHP is on average enriched in Li, Zn, Nb, Sn and Ta compared to that in the host mica schist, which is enriched in V, Cr, Co, Ni and ΣLREE relative to that in the AHP (ESM Table S15). Coarse-grained tourmaline from the AHP shows compositional variability with decreasing Be, Ti and ΣLREE and increasing Li, Nb, Sn and Ta from core to rim.

Beryl, chrysoberyl and cordierite

Beryl and chrysoberyl were analyzed for major element compositions. All beryl contains similar concentrations of SiO_2, Al_2O_3 and near stoichiometric BeO (13.4–14 wt.%) (ESM Tables S16). Analysis of beryl from the AHP shows higher mean concentrations of FeO, Na_2O and Cs_2O than in beryl from the MHP. Zoned beryl from the AHP (Fig. 3G) shows decreasing FeO, MgO and Na_2O content from core to mantle and decreasing Na_2O from mantle to rim. Beryl from both pegmatite types contains mean concentrations of Li > 1,000 ppm, Ti and Rb in the hundreds ppm, and B, P, Cr and Ga in the tens ppm (ESM Table S17). Beryl from the AHP is enriched in Mg (~ 500 ppm) relative to that in the MHP (~ 20 ppm).

Chrysoberyl from the MHP contains minor FeO (0.17–1.93 wt.%), and Ti (0.05–0.26 wt.% TiO_2) and Ca (0.08–0.21 wt.% CaO) were also detected in individual analyses (ESM Table S18). Although some chrysoberyl grains show brighter and darker intensities in BSE images (Fig. 4H), no compositional variation could be detected via EPMA.

Cordierite intergrown with quartz is considered to be an exsolution product of beryl due to its fine-grained, aligned morphology and restriction to the cores of beryl grains (Fig. 4A, F). Cordierite compositions are characterized by high MnO (2.48–2.85 wt.%), Na_2O (1.55–1.81 wt.%), X_{Fe} values of 0.83–0.85, and low SiO_2 (~ 46.5 wt.%) and Al_2O_3 (~ 29.3 wt.%) (ESM Table S19). The high Na and low Al contents in cordierite suggest the presence of BeO following the substitution $Na^+ + Be^{2+} = Al^{3+}$ (Černý and Povondra 1966; Povondra and Langer 1971). Approximately 1.0 wt.% BeO is estimated based on a regression line of BeO versus Al_2O_3 versus Na_2O by Konzett et al. (2018a, refer to Fig. 16A of same publication). Because this estimation produces high T-site ($Si + Al + Be_{calc}$) totals (~ 9.16 *apfu*), it is possible that Na only partially contributed to the substitution $Na^+ + Be^{2+} = Al^{3+}$ while excess Na substituted into the M-site (Fe, Mg, Mn) along with Li following the substitution $Li^+ + Na^+ = R^{2+}$ (Gordillo et al. 1985). This would explain low M-site totals of ~ 1.6 *apfu*. High H_2O contents are also indicated by low totals of ~ 94–95 wt.%.

Discussion

Implications for pegmatite-melt source

Chondrite-normalized REY fractionation patterns of both NFY- and LCT-type pegmatite have been compared to their host rocks to assess the validity of formation from direct anatexis (Simmons et al. 2016; Webber et al. 2019; Gion et al. 2021). For example, similarities between the fractionation patterns of LCT pegmatite and its metasedimentary and migmatitic host rocks, and a lack of possible parental plutons as a melt source have led to the hypothesis that pegmatite in the Oxford County pegmatite field (Maine, USA) formed as a result of decompression anatectic melting during

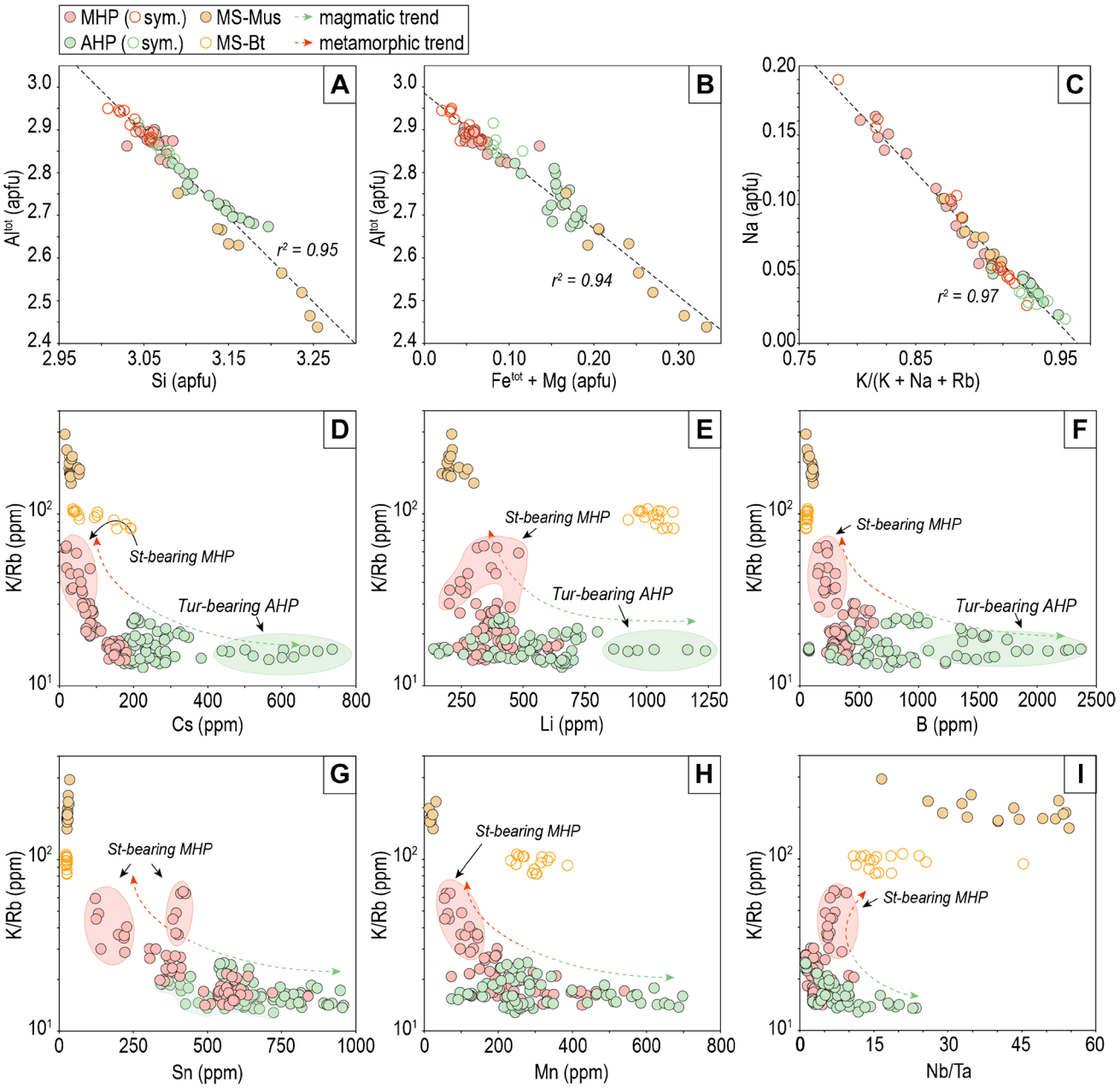

Fig. 8 Muscovite compositional data from AHP, MHP and host mica schist plotted on (**A**) Si versus Al^{tot}, (**B**) $Fe^{tot}+Mg$ versus Al^{tot} and (**C**) K/(K + Na + Rb) versus Na diagrams showing strong negative correlations. Solid circles represent magmatic and aligned muscovite from AHP and MHP, respectively, while hollow circles represent muscovite in symplectites with quartz. Binary plots for K/Rb versus (**D**) Cs; (**E**) Li (**F**) B; (**G**) Sn; (**H**) Mn; and (**I**) Nb/Ta in magmatic and aligned muscovite from AHP and MHP. Data for muscovite and biotite from host mica schist included for comparison. Abbreviations: AHP-amphibolite-hosted pegmatite; Bt-biotite; MHP-mica schist-hosted pegmatite; Mus-muscovite; MS-mica schist; Tur-tourmaline; St-staurolite; Sym-symplectic muscovite

post-orogenic extension (Simmons et al. 2016; Webber et al. 2019). A similar model is proposed for pegmatite in the AUPP (Thöni and Miller 2000; Konzett et al. 2018a, 2018b; Schuster et al. 2019; Knoll et al. 2023).

At Wolfsberg, both the AHP and the MHP display REY fractionation patterns that strongly resemble that of the host mica schist (Fig. 7B). The main differences between the REY patterns of the two pegmatite types and the host mica schist is the degree of slope and mean ΣREY, although there is much overlap between the two. The distinct negative Eu-anomaly of the mica schist is also present within the MHP, and although the AHP has an average positive Eu-anomaly, this also varies within the dataset where there also exist strong negative Eu-anomalies. Low ΣREY and inconsistent

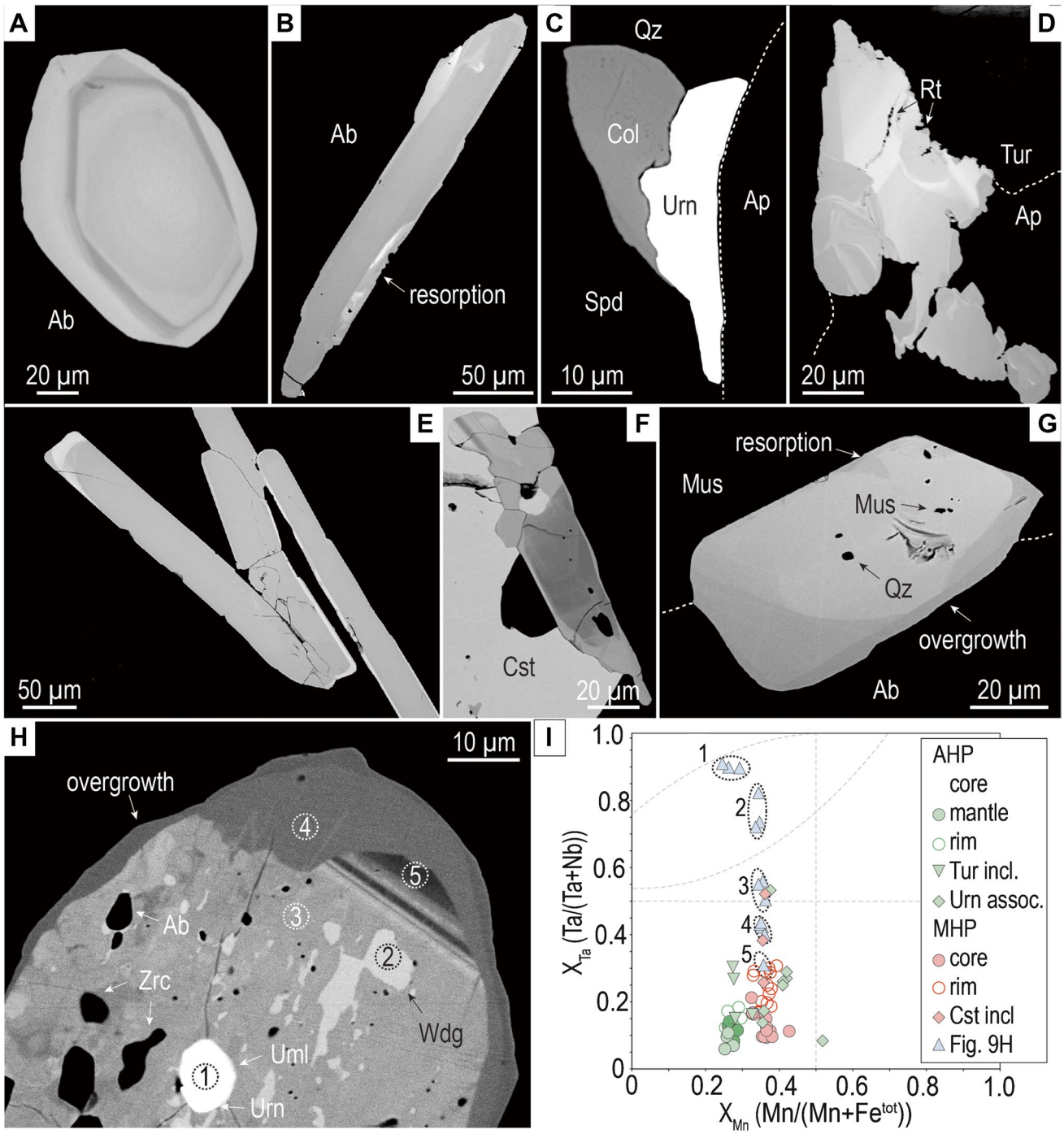

Fig. 9 BSE images showing representative textures of columbite group minerals from (**A**-**D**) amphibolite-hosted pegmatites and (**E**-**H**) mica schist-hosted pegmatites. (**A**) Columbite with core-mantle-rim texture. (**B**) Elongated lath shaped columbite with resorbed margins (white arrow). (**C**) Columbite associated with uraninite and apatite. (**D**) Columbite inclusion in tourmaline showing complex zoning features (also in Fig. 3H inset). (**E**) Columbite laths with dark cores and bright margins showing sharp zoning. (**F**) Columbite on the margin of cassiterite showing core-rim zoning. (**G**) Columbite inclusion in aligned muscovite showing a bright core, grey resorbed margins and dark overgrowths with sharp contacts. (**H**) Complex zoning in columbite with abundant inclusions of zircon, albite uraninite and uranmicrolite (also in Fig. 4I). (**I**) Compositions of CGM and wodginite plotted in terms of X_{Mn} versus X_{Ta}. Circled analyses correspond to numbers in (**H**). Abbreviations: Ab-albite; Ap-apatite; Col-columbite; Cst-cassiterite; Rt-rutile; Spd-spodumene; Tur-tourmaline; Uml-uranmicrolite; Urn-uraninite; Wdg-wodginite; Zrc-zircon

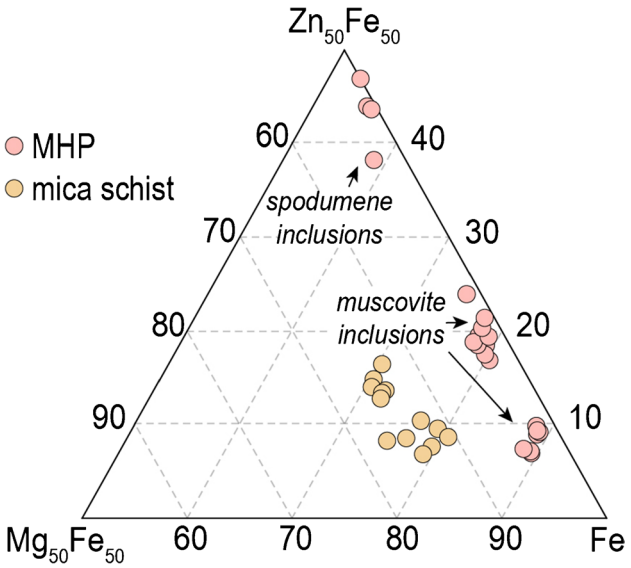

Fig. 10 Major element composition of staurolite plotted on a Mg-Zn-Fe ternary diagram

Eu-anomalies of the AHP relative to the MHP and the mica schist may be attributable to fluid-rock interaction with the amphibolite host rock where REE-rich minerals are present, such as garnet or tourmaline. Overall, from a geochemical perspective, similar peraluminous compositions and REY patterns of pegmatite to the host mica schist suggests derivation from partial melting of basement mica schist at deeper crustal levels. Contrastingly, the amphibolite host rock displays relatively flat fractionation patterns that lack resemblance to either pegmatite type or to the mica schist.

Staurolite is the most Li-rich phase in amphibolite grade metapelitic rocks (Dutrow et al. 1986). The presence of staurolite in the Al-rich metapelitic host rocks has been a key piece of evidence in models suggesting anatectic origin for spodumene pegmatite in the Eastern Alps (Konzett et al. 2018b; Schuster et al. 2019; Knoll et al. 2023). Staurolite from the mica schist has a mean Li concentration of 2,800 ppm (ESM Table S13). Of the micas within both pegmatite types and the host mica schist, biotite from the mica schist has the highest mean Li concentration of 1,030 ppm (Fig. 8E). Considering the significantly larger modal abundance of biotite relative to staurolite in the mica schist, and assuming an anatectic origin for pegmatite, biotite from the host mica schist was likely a larger contributor of Li to the pegmatite-forming melt than staurolite. Although there is no direct evidence for biotite breakdown during the Permian event, PT estimates by Krenn et al. (2021) are above the solidus for granite.

Paragenetic sequence

Petrographic observations coupled with mineral chemical analysis provide an outline for a paragenetic sequence in which the mineral associations observed within the Wolfsberg pegmatite types are attributable to two distinct events: the Permian magmatic crystallization event and the Alpine eclogite-facies metamorphism. Figure 12A outlines the key differences observed between the two pegmatite types and Fig. 12B outlines the general paragenetic sequence.

The Permian magmatic event

Crystallization of granitic pegmatite occurs over what is commonly known as the magmatic-hydrothermal transition (e.g., Ballouard et al. 2016), which distinguishes assemblages formed during early magmatic crystallization from those formed during later metasomatic and hydrothermal processes. The transition from a purely magmatic to a hydrothermal stage has been described as an unmixing process where the residual pegmatite-forming melt forms immiscible silicic and hydrosaline melts (Kaeter et al. 2018; Ballouard et al. 2020), which then interact with the primary mineral assemblage leading to albitization and/or greisenization. The Permian magmatic event can be interpreted in the context of the magmatic-hydrothermal transition, and is subdivided into the magmatic, magmatic-hydrothermal and hydrothermal stages below.

The early magmatic pegmatite-forming stage at Wolfsberg is characterized by Li-supersaturated conditions based on a lack of mineralogical zoning across pegmatite and the presence of Li-aluminosilicates proximal to the surrounding wallrocks (Maneta et al. 2015). This led to early crystallization of spodumene (high B, Mg, P, Ti, Sn, Cs, Nb, Ta), K-feldspar, albite, quartz and muscovite (low K/Rb, high Cs, Li, B, Rb, Sn). Interaction of the melt with the host amphibolite hampered spodumene crystallization due to formation of a holmquistite + biotite aureole by Li and K-loss, resulting in a thin aplitic border zone in the AHP consisting of albite, quartz, muscovite and tourmaline (Mg-, Mn-, Ti- and LREE-rich cores). Contemporaneous crystallization of Mn-apatite and beryl is suggested at this stage based on equilibrium grain boundaries with the major assemblage minerals, as is Nb-rich columbite. Despite its textural variability, columbite compositions follow a relatively consistent trend of increasing X_{Ta} with negligible X_{Mn} change (Fig. 9) that is observed in other lithium pegmatite regions, such as Namibia (Fuchsloch et al. 2019), Spain (Llera et al. 2019) and Zimbabwe (Shaw et al. 2022). This trend is suggested

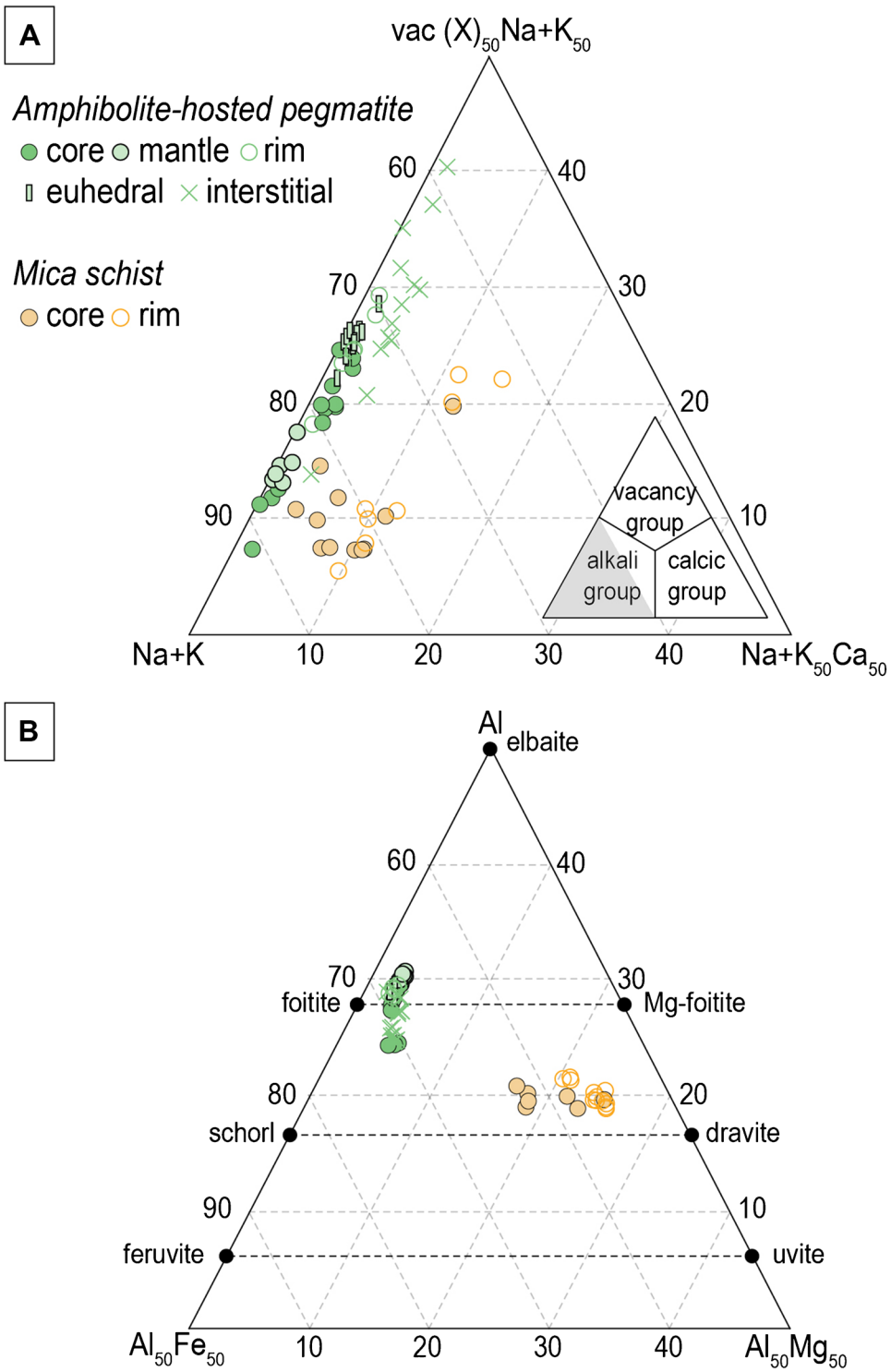

Fig. 11 Major element composition of tourmaline plotted on (**A**) Na + K-X-vacancy-Ca and (**B**) Fe-Al-Mg ternary diagrams

to be controlled by the fluorine activity of the melt, with low F activity promoting Mn-poor columbite compositions while X_{Ta} continues to increase with fractionation (Černý et al. 1986; Wise et al. 2012). A lack of F-bearing phases at Wolfsberg indicates a F-poor pegmatite-forming melt. The dominant fluid of this stage is suggested to be a mixture of magmatic, low-saline aqueous, and host rock-derived metamorphic, carbonic, fluids, based on fluid inclusion studies on garnet, tourmaline, quartz and spodumene from pegmatite in the Koralpe area by Krenn et al. (2021). The same authors obtained tourmaline fluid entrapment conditions of 4.5–5.5 kbar at 650–750 ˚C, which were interpreted as minimum pegmatite crystallization conditions, consistent with crystallization within the

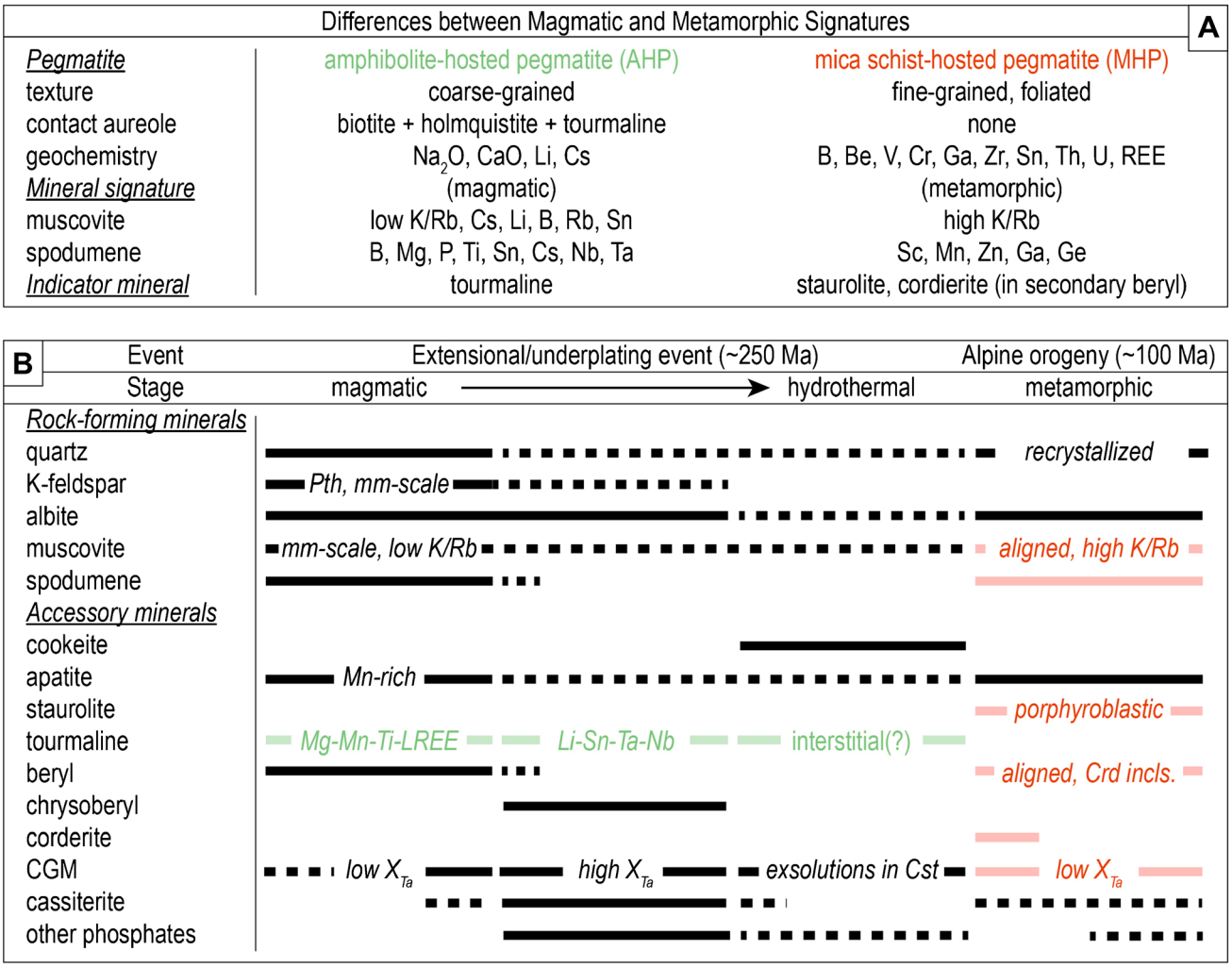

Fig. 12 **A** Textural and chemical differences between the two pegmatite types at the Wolfsberg deposit. **B** Paragenetic sequence for pegmatite. Black lines/text are characteristics observed in both pegmatite types while green and red lines/text are indicative of characteristics specific to either AHP or MHP, respectively. Textural features and trace elements definitive of a particular mineral generation are written in italics within the lines. Abbreviations: Brl-beryl; Pth-perthite; Spd-spodumene

spodumene stability (> 1.7 kbar/ < 720 ˚C; London 2005) with no evidence of prior Li-phases.

During the magmatic-hydrothermal stage, in addition to Na, concentrations of Li, Cs, Sn, Ta and Nb are expected to increase within the system. Fluids exsolved from Na-rich melts during late pegmatite crystallization have also been associated with replacement of Nb-rich columbite by Ta-richer compositions (Llera et al. 2019; Shaw et al. 2022). This could explain the observed columbite zoning trends of increasing X_{Ta}, either as normal zoning to more Ta-rich compositions (Fig. 9E) or resorption of earlier Nb-rich compositions and growth of Ta-richer compositions (Fig. 9B). However, oscillatory or patchy zoning in columbite may be indicative of temporal disequilibrium within the system (Van Lichtervelde et al. 2018). Crystallization of tourmaline rims (Li-, Sn-, Ta-, Nb-rich), cassiterite, chrysoberyl and various phosphates is interpreted to have occurred during this stage.

Albitization may have continued into the late hydrothermal stage based on the presence of albite veinlets crosscutting platy albite associated with the albitization of K-feldspar and spodumene (Fig. 3C, D). Further hydrothermal activity is evidenced by incipient cookeite replacement of spodumene, phosphate veining and grain boundary fluid migration shown by muscovite + quartz symplectites at K-feldspar and muscovite interfaces. Tourmaline interstitial to albite may suggest excess B in late hydrothermal fluids. Columbite-cassiterite associations, such as those in Fig. 4G, have been described by Konzett et al. (2018a) and were interpreted as resulting from columbite exsolution from Nb–Ta-rich cassiterite during post-magmatic cooling, which may be assigned to this stage.

The Alpine metamorphic event

This stage is represented by minerals found within the foliation of MHP and indicates element remobilization. The foliation assemblage includes recrystallized quartz, albite, muscovite, spodumene and staurolite. Lower concentrations of highly mobile elements Li, B, Cs, Sn and Rb in metamorphic muscovite and spodumene suggests remobilization/loss of these elements during (re)crystallization. Staurolite has been reported in pegmatite from other regions in the Eastern Alps and was interpreted as resulting from magmatic crystallization (Konzett et al. 2018b). However, at Wolfsberg, staurolite is included in aligned muscovite and is clearly metamorphic in origin. Crystallization of Li-rich (> 4,000 ppm) staurolite porphyroblasts and coarse-grained beryl within the foliation (Fig. 4A, E, F) is indicative of Li availability during foliation development. Lithium was likely mobile in solution considering the presence of aqueous high-saline metamorphic fluids during the Alpine metamorphism, as suggested by fluid inclusions in recrystallized quartz from pegmatites of the Koralpe (Krenn et al. 2021). Metamorphic fluids are suggested to have derived from decompression melting/dehydration of host metapelite in the area during the Alpine metamorphism and have also resulted in local pegmatite formation (Thöni and Miller 2010; Schorn et al. 2021). Apatite, beryl (with quartz + cordierite exsolutions), and Nb-rich columbite either as overgrowths on grains included in aligned muscovite (Fig. 9G) or within metamorphic beryl or staurolite (Fig. 4A, F), are also attributable to the metamorphic stage and suggest mobility of Be, Nb and Ta during foliation development.

Conclusions

The relationship between petrography and trace element chemistry of minerals from the two pegmatite types at the Wolfsberg deposit show that, although their emplacement is temporally tied to the same Permian event, they display mineralogical and chemical differences that result from different melt-host rock interactions and different host rock rheology during the Alpine orogeny. Trace element compositions of minerals from the AHP, such as coarse-grained muscovite and spodumene, show it has retained highly fractionated magmatic chemical signatures, whereas the texture and composition of minerals within the MHP, including aligned muscovite and spodumene, reflects recrystallization during metamorphism. Geochemical similarities between chondrite-normalized REY fractionation patterns of the host mica schist and pegmatite supports an anatectic origin for pegmatite via melting of mica schist host rock, comparable to metapelite-derived pegmatite elsewhere. Although metasomatic processes such as albitization occurred during initial pegmatite emplacement, later metasomatic element remobilization within pegmatite occurred during decompression fluid release following the Alpine orogeny, which was especially important in the MHP. Recognition of element remobilization, particularly Li and Cs, in the MHP associated with metamorphic overprinting may bear important implications towards mineral exploration for LCT pegmatite in other strongly metamorphosed terranes.

Supplementary Information The online version contains supplementary material available at https://doi.org/10.1007/s00126-023-01176-w.

Acknowledgements Logistical support and mine access from European Lithium Limited and sampling assistance from geologists at GEO-Unterweissacher GmbH is greatly appreciated. Constructive reviews by K. Goodenough and Associate Editor Romer helped to improve the manuscript.

Funding Open access funding provided by University of Oslo (incl Oslo University Hospital) This is a contribution to project GREEN-PEG-New Exploration Tools for European Pegmatite Green-Tech Resources, supported by the Horizon 2020 Framework Programme of the European Union (grant number EU H2020 GA869274).

Declarations

Conflict of interest The authors have no competing interests to declare.

References

Ballouard C, Poujol M, Boulvais P, Branquet Y, Tartèse R, Vigneresse J (2016) Nb-Ta fractionation in peraluminous granites: a marker of the magmatic-hydrothermal transition. Geology 44:231–234

Ballouard C, Elburg MA, Tappe S, Reinke C, Ueckermann H, Doggart S (2020) Magmatic-hydrothermal evolution of rare metal pegmatites from the Mesoproterozoic Orange River pegmatite belt (Namaqualand, South Africa). Ore Geol Rev 116:103252

Černý P, Ercit TS (2005) The classification of granitic pegmatites revisited. Can Mineral 43:2005–2006

Černý P, Povondra P (1966) Beryllian cordierite from Věžná: (Na, K) + Be → Al. Neues Jahrbuch Für Mineralogie Monatsh 44:36–44

Černý P, Goad BE, Hawthorne FC, Chapman R (1986) Fractionation trends of the Nb- and Ta-bearing oxide minerals in the Greer Lake pegmatitic granite and its pegmatite aureole, southeastern Manitoba. Am Miner 71:501–517

Dutrow BL, Holdaway MJ, Hinton RW (1986) Lithium in staurolite and its petrologic significance. Contrib Miner Petrol 94:496–506

European Lithium Limited (2021) Interim financial report for the half year ended 31 December 2021. https://europeanlithium.com/wp-content/uploads/2022/02/220216-EUR-HY22-Half-Year-Report-31-Dec-2021-FINAL.pdf

Fuchsloch WC, Nex PAM, Kinnaird JA (2019) The geochemical evolution of Nb-Ta-Sn oxides from pegmatites of Cape Cross-Uis pegmatite belt, Namibia. Mineral Mag 83:161–179

Gangl S, Piber A, Tropper P, Klötzli U, Finger F, Mirwald PW (2005) Geochronological evidence for lower Ordovician magmatism in the crystalline nappes north of the Tauern Window. Geophys Res Abstr 7:03975

Gion AM, Piccoli PM, Fei Y, Candela PA, Ash RD (2021) Experimental constraints on the formation of pegmatite-forming melts by anatexis of amphibolite: a case study from Evje-Iveland. Norway Lithos 398–399:106342

Göd R (1989) The spodumene deposit at "Weinebene", Koralpe, Austria. Miner Deposita 24:270–278

Gordillo CE, Schreyer W, Werding G, Abraham K (1985) Lithium in NaBe-cordierites from El Peñón, Sierra de Córdoba, Argentina. Contrib Miner Petrol 90:93–101

Gourcerol B, Gloaguen E, Melleton J, Tuduri J, Galiegue X (2019) Re-assessing the European lithium resource potential – a review of hard-rock resources and metallogeny. Ore Geol Rev 109:494–519

Habler G, Thöni M, Miller C (2007) Major and trace element chemistry and Sm-Nd age correlation of magmatic pegmatite garnet overprinted by eclogite-facies metamorphism. Chem Geol 241(1):4–22

Heede HU (1997) Isotopengeologische Untersuchungen an Gesteinen des ostalpinen Saualpenkristallins, Kärnten–Österreich. Münstersche Forschungen zur Geologie und Paläontologie 81:1–168

Kaeter D, Barros R, Menuge JF, Chew DM (2018) The magmatic–hydrothermal transition in rare-element pegmatites from southeast Ireland: LA-ICP-MS chemical mapping of muscovite and columbite– tantalite. Geochim Cosmochim Acta 240:98–130

Kavanagh L, Keohane J, Cabellos GG, Lloyd A, Cleary J (2018) Global lithium sources-Industrial use and future in the electric vehicle industry: a review. Resources 7:57. https://doi.org/10.3390/resources7030057

Kesler SE, Gruber PW, Medina PA, Keoleian GA, Everson MP, Wallington TJ (2012) Global lithium resources: relative importance of pegmatite, brine and other deposits. Ore Geol Rev 48:55–69

Knoll T, Schuster R, Huet B, Mali H, Onuk P, Horschinegg M, Ertl A, Giester G (2018) Spodumene pegmatites and related leucogranites from the Austroalphine Unit (eastern Alps, central Europe): field relations, petrography, geochemistry, and geochronology. Can Mineral 56:489–528

Knoll T, Huet B, Schuster R, Mali H, Ntaflos T, Hauzenberger C (2023) Lithium pegmatite of anatectic origin - A case study from the Austroalpine Unit Pegmatite Province (Eastern European Alps): geological data and geochemical model. Ore Geol Rev 154:105298

Konzett J, Schneider T, Nedyalkova L, Hauzenberger C, Melcher F, Gerdes A, Whitehouse M (2018a) Anatectic Granitic Pegmatites from the Eastern Alps: A case of variable rare-metal enrichment during high-grade regional metamorphism – I: mineral assemblages, geochemical characteristics, and emplacement ages. Can Mineral 56:555–602

Konzett J, Hauzenberger C, Ludwig T, Stalder R (2018b) Anatectic granitic pegmatites from the eastern alps: A case of variable rare metal enrichment during high-grade regional metamorphism. II: Pegmatite staurolite as an indicator of anatectic pegmatite parent melt formation – a field and experimental study. Can Mineral 56:603–624

Krenn K, Husar M, Mikulics A (2021) Fluid and solid inclusions in host minerals of Permian pegmatites from Koralpe (Austria): deciphering the Permian fluid evolution during pegmatite formation. Minerals 11:638. https://doi.org/10.3390/min11060638

Llera AR, Fuertes-Fuenta M, Cepedal A, Martin-Izard A (2019) Barren and Li-Sn-Ta mineralized pegmatites from NW Spain (central Galicia): a comparative study of their mineralogy, geochemistry, and wallrock metasomatism. Minerals 9:739. https://doi.org/10.3390/min9120739

London D (2005) Geochemistry of alkali and alkaline earth elements in ore-forming granites, pegmatites and rhyolites. In: Linnen RL, Samson IM (Eds.), Rare element geochemistry and mineral deposits. Geological Society of Canada Short Course Notes 17:17–44

London D (2008) Pegmatites. Canadian Mineralogist Special Publication 10:368 p

Mali H (2004) Die spodumenpegmatite von Bretstein und Pusterwald (Wölzer Tauren, Steiermark, Österreich). Joannea Mineralogie 2:5–53

Mandl M, Kurz W, Hauzenberger C, Fritz H, Klötzli U, Schuster R (2018) Pre-Alpine evolution of the Seckau Complex (Austroalpine basement / Eastern Alps): Constraints from in-situ LA-ICP-MS U-Pb zircon geochronology. Lithos 296–299:412–430

Maneta V, Baker DR, Minarik W (2015) Evidence for lithium-aluminosilicate supersaturation of pegmatite-forming melts. Contrib Miner Petrol 170:1–16

McDonough WF, Sun S-s (1995) The composition of the Earth. Chem Geol 120:223–253

Miller C, Thöni M (1997) Eo-Alpine eclogitisation of Permian MORB-type gabbros in the Koralpe (Eastern Alps, Austria): new geochronological, geochemical and petrological data. Chem Geol 137:283–310

Miller C, Thöni M, Konzett J, Kurz W, Schuster R (2005) Eclogites from the Koralpe and Saualpe type localities, Eastern Alps, Austria. Mitt Österr Mineral Ges 150:227–263

Morauf W (1980) Die permische differentiation und due alpidische metamorphose des granitgneises von Wolfsberg, Koralpe, SE-Ostalpen, mit Rb-Sr- und K-Ar-isotopenbestimmungen. Tschermaks Mineralogische Und Petrographische Mitteilungen 27:169–185

Niedermayr VG, Göd R (1992) Das spodumenvorkommen auf der Weinebene und seine mineralien. Carinthia II 182:21–35

Povondra P, Langer K (1971) Synthesis and some properties of sodium-beryllium-bearing cordierite Na_x-$Mg_2Al_{4-x}Be_xSi_5O_{18}$). Neues Jb Mineral Abh 113:1–19

Rudnick RL, Gao S (2004) Composition of the continental crust. Treatise Geochem 3:1–64

Schmid SM, Fügenschuh B, Kissling E, Schuster R (2004) Tectonic map and overall architecture of the Alpine orogen. Eclogae Geologicase Helvetiae 97:93–117

Schorn S, Hartnday MIH, Diener JFA, Clark C, Harris C (2021) H_2O-fluxed melting of eclogite during exhumation: an example from the eclogite type-locality, Eastern Alps (Austria). Lithos 390–391:106118

Schuster R, Stüwe K (2008) Permian metamorphic event in the Alps. Geology 36:303–306

Schuster R, Scharbert S, Abart R, Frank W (2001) Permo-Triassic extension and related HT/LP metamorphism in the Austroalpine-Southalpine realm. Mitteilungen Der Gesellschaft Der Geologie Und Bergbaustudenten Österreichs 44:111–141

Schuster R, Huet B, Knoll T, Paulick H (2019) Anatectic origin of albite-spodumene pegmatites: a geochemical model. Geophys Res Abstr 21:EGU2019-7277

Shaw RA, Goodenough KM, Deady E, Nex P, Ruzvidzo B, Rushton JC, Mounteney I (2022) The magmatic-hydrothermal transition in lithium pegmatites: petrographic and geochemical characteristics of pegmatites from the Kamativi area, Zimbabwe. Can Mineral 60:1–31

Shaw RA (2021) Global lithium (Li) mines, deposits and occurrences (November 2021). Brit Geol Surv. https://www2.bgs.ac.uk/mineralsuk/download/global_critical_metal_deposit_maps/G2122_052_V4CMYK.pdf

Simmons W, Falster A, Webber K (2016) Bulk composition of Mt. Pegmatite, Maine USA: implications for the origin of an LCT type pegmatite by anatexis. Can Mineral 54:1053–1070

Sweetapple MT (2017) A review of the setting and internal characteristics of lithium pegmatite systems of the Archean North Pilbara and Yilgarn Cratons, Western Australia. Granites 2017@Benalla Symposium, Victoria, Australia. Ext Abstr AIG Bull 65:113–117

Thöni M, Miller C (2000) Permo-Triassic pegmatites in the eo-Alpine eclogite-facies Koralpe complex, Austria: age and magma source constraints from mineral chemical, Rb-Sr and Sm-Nd isotope data. Schweiz Mineral Petrogr Mitt 80:169–186

Thöni M, Miller C (2004) Ordovician meta-pegmatite garnet (N-W Ötztal basement, Tyrol, Eastern Alps): preservation of magmatic garnet chemistry and Sm-Nd age during mylonitization. Chem Geol 209:1–26

Thöni M, Miller C (2010) Andalusite formation in a fast exhuming high-P wedge: textural, microchemical, and Sm-Nd and Rb-Sr age constraints for a Cretaceous P-T-t path at Kienberg, Saualpe (Eastern Alps). Austrian J Earth Sci 103(2):118–131

Tropper P, Finger F, Krenn E, Klötzli U, Piber A, Gangl S (2016) The Kellerjoch Gneiss (Tyrol, Eastern Alps): An Ordovician pluton with A-type affinity in the crystalline basement nappes north of the Tauern Window. Austr J Earth Sci 109:178–188

Van Lichtervelde M, Holtz F, Melcher F (2018) The effect of disequilibrium crystallization on Nb-Ta fractionation in pegmatites: constraints from crystallization experiments in tantalite-tapiolite. Am Miner 103:1401–1416

Webber KL, Simmons WB, Falster AU, Hanson SL (2019) Anatectic pegmatites of the Oxford County pegmatite field, Maine, USA. Can Mineral 57:811–815

Wise MA, Francis CA, Černý P (2012) Compositions and structural variations in columbite-group minerals from granitic pegmatites of the Brunswick and Oxford fields, Maine: differential trends in F-poor and F-rich environments. Can Mineral 50:1515–1530